

AD-A148 339

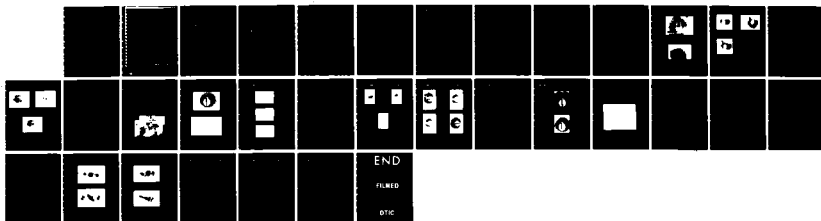
HOLOGRAPHIC FLI FOR DETECTION OF DEFECTS(U) HONEYWELL  
ELECTRO-OPTICS DIV LEXINGTON MA G O REYNOLDS ET AL.  
JUL 84 8309-38 AFOSR-TR-84-0976 F49620-82-C-0001

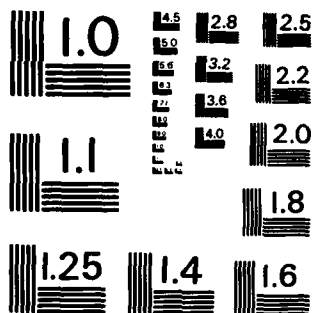
1/1

UNCLASSIFIED

F/G 20/6

NL





MICROCOPY RESOLUTION TEST CHART  
NATIONAL BUREAU OF STANDARDS-1963-A

(4)

AD-A148 339

# HOLOGRAPHIC FLI FOR DETECTION OF DEFECTS

## INTERIM REPORT

*July 1984*

Contract #F49620-82-C-0001

DTIC  
ELECTE  
DEC 07 1984  
S  
E

Approved for public release;  
distribution unlimited.

DTIC FILE COPY

# Honeywell

84 11 20 06 9

# **HOLOGRAPHIC FLI FOR DETECTION OF DEFECTS**

## **INTERIM REPORT**

**Contract #F49620-82-C-0001**

***July 1984***

**AIR FORCE OFFICE OF SCIENTIFIC RESEARCH (AFOSR)**

**NOTICE OF TRANSMITTAL TO DTIC**

**This technical report is approved for public release and is approved for distribution under E.O. 13526-12. Distribution is unlimited.**

**MATTHEW J. KERNER**

**Chief, Technical Information Division**

**Honeywell**

**ELECTRO-OPTICS DIVISION  
2 FORBES ROAD  
LEXINGTON, MA 02173**

UNCLASSIFIED

SECURITY CLASSIFICATION OF THIS PAGE (When Data Entered)

REPORT DOCUMENTATION PAGE		READ INSTRUCTIONS BEFORE COMPLETING FORM
1. REPORT NUMBER <b>AFOSR-TR- 84 - 0976</b>	2. GOVT ACCESSION NO.	3. RECIPIENT'S CATALOG NUMBER
4. TITLE (and Subtitle) <b>Holographic FLI For Detection of Defects</b>		5. TYPE OF REPORT & PERIOD COVERED <b>Interim Jan. 15, 1984 July 1, 1984</b>
6. AUTHOR(s) <b>George O. Reynolds, P.I., Donald A. Servaes, Luis Ramos, Honeywell EOD; Daniel Pierce, Ronald Mayville, Peter Hilton, Arthur D. Little, Inc., John B. DeVelis, Merrimack Col.</b>		8. PERFORMING ORG. REPORT NUMBER <b>8309-38</b>
7. PERFORMING ORGANIZATION NAME AND ADDRESS <b>Honeywell, Electro-Optics Division 2 Forbes Road Lexington, MA 02173</b>		9. CONTRACT OR GRANT NUMBER(s) <b>F49620-82-C-0001</b>
11. <b>AFOSR/NA Bellingham AFB, DC-20332</b>		10. PROGRAM ELEMENT PROJECT, TASK AREA & WORK UNIT NUMBERS <b>61102F, 2306, A2</b>
12. MONITORING AGENCY NAME & ADDRESS (if different from Controlling Office)		12. REPORT DATE <b>July 1984</b>
		13. NUMBER OF PAGES
		14. SECURITY CLASS (of this report) <b>NA</b>
		15a. DECLASSIFICATION/DOWNGRADING SCHEDULE <b>NA</b>
16. DISTRIBUTION STATEMENT (of this Report)  <b>NA</b> <span style="float: right;">Approved for public release; distribution unlimited.</span>		
17. DISTRIBUTION STATEMENT (of the abstract entered in Block 20, if different from Report)  <b>NA</b>		
18. SUPPLEMENTARY NOTES  <b>NONE</b>		
19. KEY WORDS (Continue on reverse side if necessary and identify by block number)  <b>Holographic Interferometry, Non-Destructive Evaluation, Lasers Moire Techniques, Finite Element Analyses</b> <span style="float: right;">(Fringe linearization interferometry)</span>		
20. ABSTRACT (Continue on reverse side if necessary and identify by block number) <b>contract #F49620-82-C-0001</b> In this interim report, we show that the two-exposure FLI holographic method is feasible. We briefly review the state-of-the-program prior to this reporting period. We describe the series of experiments and mathematical modeling which led to the development of a new test plate fixture, and the introduction of the four-exposure Moire method. We then describe how the original two-exposure FLI technique can be utilized by increasing the linear fringe frequency. We also describe a two wavelength method for the four-exposure		

DD FORM 1, JAN 73 1473 EDITION OF 1 NOV 65 IS OBSOLETE

UNCLASSIFIED

SECURITY CLASSIFICATION OF THIS PAGE (When Data Entered)

(over)

UNCLASSIFIED

20. ABSTRACT (cont'd)

*cont* → FLI Moire method which leads to a desensitization. The feasibility of an automatic readout for the linear fringe method is demonstrated by showing that observable and measurable effects at the defect site can be monitored. Finally, we outline the remaining program. ↗

UNCLASSIFIED

## SECTION 1 INTRODUCTION

### 1.1 PROGRESS

This interim report for contract #F49620-82-C-0001 demonstrates that the Holographic FLI concept is feasible. This is based on experimental results and model calculations using static loading. We will show how the results obtained through experimentation and mathematical modeling and presented in the two previous annual reports (April 1983, April 1984) led to a re-examination of the original FLI concept from a different perspective, which lead to the results presented in this report. The first results came from the recognition that a new static fixture for applying the load to the test plate with a through crack and a hidden crack was necessary to detect the presence of the defect as predicted in the modeling work. Use of this new fixture led immediately to the success of the holographic FLI as suggested in the original proposal.

The previous results demonstrated a desensitization with a moire technique obtained from a four-exposure hologram. This enables the stated condition of a deformation limit of one quarter wave of deformation per linear fringe cycle to be met. This condition is also satisfied by increasing the linear fringe frequency.

### 1.2 CONTRIBUTORS TO THE REPORT

This study's principal investigator is George O. Reynolds from the Honeywell Electro-Optics Division. Donald A. Servaes, the Project Experimentalist, and Luis Ramos, the Experimental Assistant, are also from Honeywell. Dr. John B. DeVelis, a consultant to Honeywell from Merrimack College, has contributed to the study. Ronald A. Mayville, Peter D. Hilton and Daniel C. Peirce from Arthur D. Little, Inc. under a subcontract performed mechanical designs, modeling work and deformation analysis.

Accession For	
NTIS GRA&I	<input checked="" type="checkbox"/>
DTIC TAB	<input type="checkbox"/>
Unannounced	<input type="checkbox"/>
Justification	
By	
Distribution/	
Availability Codes	
Avail and/or	
Dist	Special

**A-1**

## **SECTION 2 RESEARCH OBJECTIVE**

The objective of this program's research is to prove the concept of Holographic Fringe Linearization Interferometry (FLI) and determine its degree of utility. In the FLI technique, linear fringes are introduced in the formation step of double exposure holographic interferometry by using a beam deflector in the object beam between two holographic exposures.

The addition of the linear fringe of the appropriate spatial frequency to the interferogram dominates the random fringes that commonly appear in double exposure holography. The superposition of the linear fringes with the random fringes yields a pattern, that is comprised of straight line fringes everywhere except at the defect region.

The goal of this research program is the experimental demonstration of the FLI technique for

detecting and locating (not necessarily identifying or classifying) subsurface cracks and defects in various structures. Since FLI is a potentially large area inspection technique that is compatible with image processing, its success can simplify the Nondestructive Evaluation (NDE) process for large military structures such as aircraft.

The experimental work to date has been performed by Honeywell at the Electro-Optics Division, Advanced Concepts Group in Wilmington, MA. Initial experimentation at NADC was performed. We do not anticipate performing any more work at NADC during the remainder of the program. Modeling work and deformation analysis was performed at Arthur D. Little, Inc. in Cambridge, MA.

## SECTION 3 PROGRESS, PRELIMINARY RESULTS AND PLANS

The FLI program is scheduled to be a three-phase study during a three-year period. This report discusses work performed and results obtained during the first half of Phase III.

During this reporting period, we experimentally located a subsurface crack with the FLI technique. We used a load fixture that was designed to stress the test plate the same way the computer model plate was stressed. The desensitization needed to remove the noise fringes characteristic of double exposure holography was realized by increasing the linear fringe frequency. If necessary, additional desensitization can be obtained using the two-color, four-exposure moire technique developed in Phase II. In addition, we have demonstrated that defects have a Fourier signature that is amenable to an automatic readout implementation.

The experiment was repeated in the computer study. A hidden defect was modeled and the plate stressed. Displacement contours were calculated and plotted. As in the experiment, the

defect location was barely suggested by the contour line bends. Linear fringes were added and the superposition of the linear fringe and the deformation contours plotted. When the linear fringe frequency was high enough to dominate the contour pattern, the defect was made visible. The computer model and the experiment are in excellent agreement.

The following outlines our plan for the remainder of the program:

1. Perform a sensitivity analysis with the computer model that will be verified experimentally;
2. Demonstrate desensitization with two-color moire FLI; and
3. Model and perform a simple dynamic loading experiment using our Argon laser and a small field-of-view.

No further experiments are planned at NADC during this program.

## SECTION 4 PROBLEMS ENCOUNTERED DURING PHASE III

### PROBLEM 1

Honeywell sold their Brighton facility and moved the project team to their plant in Wilmington, MA. The laboratory was unavailable for use from mid-November until early March.

**Solution** - Work on the project was stopped during this period to preserve project funds.

**Status** - When the new lab was opened in early March, the project team returned to their investigations.

### PROBLEM 2

During the move, the Argon Laser tube was broken, rendering the laser inoperable. Therefore, the two-color moire experiments were not completed.

**Solution** - A new tube was installed by the vendor at Honeywell's expense.

**Status** - The repaired laser is now installed in the lab. The water supply to the lab is being increased to accommodate the flow rates required by the laser cooling system. Preparations are underway to continue the two-color moire experiment.

## SECTION 5 TECHNICAL STATUS OF RESEARCH EFFORT

### 5.1 INTRODUCTION

This section reviews work done during previous phases and discusses the significant accomplishments achieved during this reporting period.

### 5.2 HOLOGRAPHIC FLI REVIEW

#### 5.2.1 Goal of Proposed Concept

The Goal of FLI is two-fold.

**Goal 1 -** Replace the complicated interference pattern obtained from two-exposure holographic interferometry used for non-destructive testing (NDT) with the simpler linear fringe pattern of FLI.

This is illustrated in Figure 5-1, taken from the original proposal. In Figure 5-1(a), we show the complicated fringe pattern from typical two-exposure holographic interferometry, in which the cracks are difficult to locate. In Figure 5-1(b), we show the results of an experiment illustrating the ease of locating a defect in a field of clean fringes.

**Goal 2 -** Use the linear fringes to ease automatic readout for defect locating over large areas.

#### 5.2.2 Vector Addition Nature of Linear Fringes in Double Exposure Holography

In Section 5 of the April 1984 Annual Report\*, a series of experiments were reported demonstrating that the linear fringes, resulting from

\*2nd Annual Report on FLI Contract, #F49620-82-C-0001 Honeywell Electro-Optics Division Report #8403-10 April 1984.

rotating the object beam between exposures of a double exposure hologram, add vectorially to the surface deformation contours caused by loading. These results were for the case of a simple deformation (object tilt about one axis) and a beam rotation about the other axis.

Figure 5-2(a) shows the linear fringes present in the reconstructed image of a double exposure hologram arising from tipping the test plate about the x-axis between exposures. Figure 5-2(b) shows linear fringes from rotating the object beam about the y-axis between exposures. Figure 5-2(c) shows the linear fringes arising from the vector addition of the linear fringes from tilting the test plate as in Figure 5-2(a) and rotating the object beam as in Figure 5-2(b). The fringes in Figure 5-2(c) are rotated through an angle. The horizontal and vertical fringes have been added vectorially to produce the rotated linear fringe pattern. Figure 5-2(c) also shows that the higher x-axis fringes due to tilting the test plate dominated the y-axis fringe from the object beam rotation when the two are vectorially added in the two-exposure hologram. Figure 5-2(d) shows the addition of two vectors along the x-axis and the y-axis resulting in the vector  $\omega$ . These experiments led to the following interpretation of the two-exposure FLI holographic equation,

$$\cos(\omega x + \Delta(x,y)) \quad (1)$$

Where  $\omega x$  represents the linear fringe and  $\Delta(x,y)$  is the out-of-plane displacement of the surface. The resulting interference pattern is the sum of the linear fringe,  $\omega x$  and the surface deformation,  $\Delta(x,y)$ .



**Figure 5-1(a). Complicated Fringe Pattern on a 48 by 25 in. Panel Using the Pulsed Holographic NDT Technique. The Areas of Stress Corrosion Cracking are Indicated by Fringe Shifts in the Boxed-in Areas (From Ref. 1).**

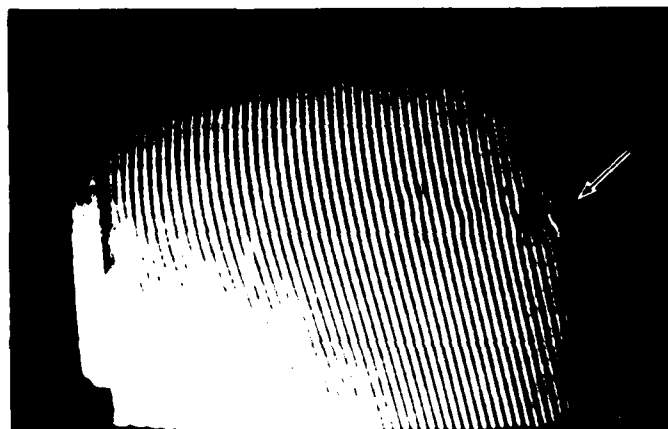


**Figure 5-1(b). Double Pulsed Holographic NDE of a 125 mm by 90 mm Defective Rubber-Steel Laminate Showing Debonding and Illustrating the Ease of Locating a Defect in a Field of Clean Fringes (From Ref. 2).**

**Figure 5-1. Comparison of Results of a Two-Exposure Holographic Interferometry NDT and the Simpler FLI Technique for Locating Defects.**

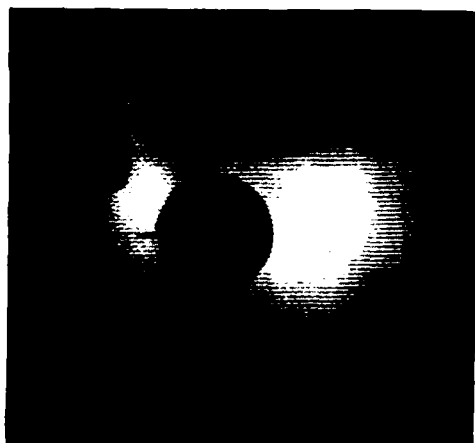


**Figure 5-2(a). Reconstructed Image of Double Exposure Hologram Resulting from Tipping the Test Plate about the x-Axis Between Exposures**

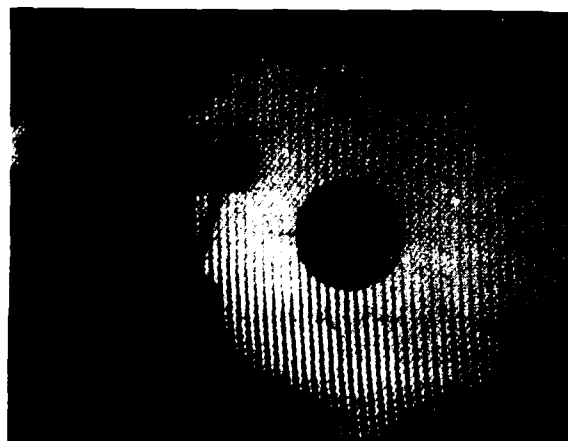


**Figure 5-2(b). Reconstructed Image of Double Exposure Hologram Resulting from Rotating the Object Beam About the y-Axis Between Exposures**



**Figure 5-2(c). Reconstructed Image of Double Exposure Hologram Resulting from Rotating the Object Beam About the y-Axis and Tipping the Test Plate About the x-Axis Between Exposures**

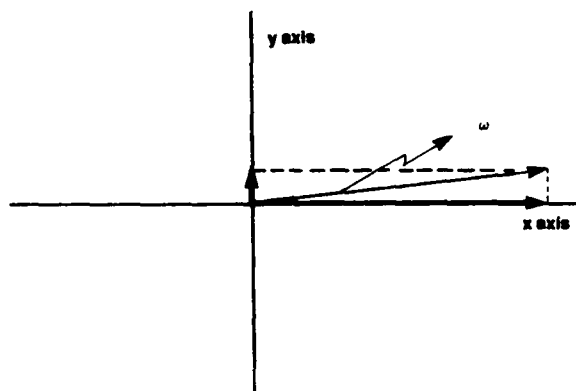


**Figure 5-2(d). Vector Addition of Linear Fringes of Different Frequencies ( $\omega_1 > \omega_2$ ).**

**Figure 5-2. Experimental Demonstration of the Vector Addition of Linear Fringes in Double Exposure Holography**

### 5.2.3 Interpretation of Vector Fringe Addition Leading to the Loading Limitation

Interpreting the experimental results demonstrated in Figure 5-2 in terms of the basic interference equation of two-exposure FLI holography, Eq(1), led to the following conclusion:

*If the out-of-plane deformation of the test plate due to differential loading between exposures that yields the  $\Delta(x,y)$  phase term in equation (1) is greater than one-quarter wavelength per linear fringe period given by the  $\omega x$  term in equation (1), then the vector addition of fringes would lead to the  $\Delta(x,y)$  term dominating the linear fringe term in equation (1). This would result in the linear fringe term being swamped by the fringes due to any differential loading, rendering the FLI concept ineffective.*

This constraint can be met in two ways: (1) fixing the fringe frequency and desensitizing the effect of the deformation by using Holographic moire techniques; or (2) increasing the fringe frequency  $\omega$  so that the spatial period is smaller than the distance over which the deformation changes by  $\lambda/4$ . This latter method was used to prove the experimental feasibility of FLI for locating subsurface defects.

### 5.2.4 Holographic Moire Technique

As discussed in Section 5 of the April, 1984 Annual Report, experiments were performed demonstrating a variation of the important work of N. Abramson in which the random fringes due to the loading were used as a carrier to recover the desired linear fringes using the moire method. It appears that this technique can be a desensitizing method to overcome the quarter wavelength per cycle restriction resulting from the loading limitation. The four-exposure FLI Moire technique was developed and the experimental procedure is described below. Notice that it consists of two consecutive double exposures.

1. The test body was hologrammed in state #1, its relaxed state. This is hologram #1.
2. The second exposure on hologram #1 was made after stressing the object by turning two thumb screws in the test fixture. This is state #2 of the object.
3. Another double exposure hologram is made. The first exposure on hologram #2 is the same as the second exposure on hologram #1, (i.e. a hologram of the surface in state #2). The same laser can be used as for hologram #1.
4. The stress is removed from the plate by loosening the thumb screws and the object beam is shifted through an angle. A hologram of state #1 with the shifted beam is made as the second exposure on hologram #2.

This experimental process was carried out to demonstrate the moire principle. A photograph of the reconstruction of the first double exposure hologram made from the first two steps of the process is shown in Figure 5-3(a). A photograph of the reconstruction of the second double exposure hologram made from steps three and four of the procedure is shown in Figure 5-3(b). Note the resulting fringe pattern in these figures due to the test object being stressed. Also, note in Figure 5-3(b) that the linear fringe due to shifting the object beam through an angle is not visible since the magnitude of the deformation is greater than one-quarter wavelength per fringe period. However, moireing the two images in Figures 5-3(a) and 5-3(b) yields the result shown in Figure 5-3(c) where the linear fringe is quite obvious. This fringe is not visible in the conventional FLI because loading restrictions have not been satisfied.

The moire (difference) technique subtracts the common random phase between the two interferograms and emphasizes the linear fringe that was present (albeit small and not visible) in one image (Figure 5-3(b)) but not the other (Figure



**Figure 5-3(a). Reconstructed Image (Holographic Interferogram) from Double Exposure Hologram #1.**



**Figure 5-3(b). Reconstructed Image (Holographic Interferogram) from Double Exposure Hologram #2. The Linear Fringe is Not Observable.**



**Figure 5-3(c). Moire of the Two Random Noise Interferograms Indicating the Presence of the Linear Fringe.**

**Figure 5-3. Demonstration of the Desensitizing Property of Holographic Moire FLI**

5-3(a)). The fact that the FLI fringes are not perfectly linear across Figure 5-3(c) means that the plate did not relax to its original position.

This successful demonstration of the desensitization property of the Holographic Moire technique led to attempts to simplify the moire procedure and to load the test specimen in a similar way to the mathematical model developed at ADL. Those investigations showed a desensitizing with increasing linear fringe frequency suggesting that the effect can be obtained with double exposure (i.e., the quarter wave per fringe period could be met by using a high enough fringe frequency). The high frequency fringes dominate the deformation due to the differential loading while showing an observable change in the linear fringes at the defect.

## 5.3 DEMONSTRATION OF HOLOGRAPHIC FLI FEASIBILITY

### 5.3.1 The New Loading Fixture

A mathematical model was developed by ADL for the two-exposure hologram. Close examination of the loading technique for the plug test plate indicated that loading for the test plate was applying forces on the defect that were not the same as those applied in the model. Therefore, a new fixture was designed to match the experiment to the model. The forces in the model are shown in Figure 5-4(a) and a photograph of the experimental apparatus is shown in Figure 5-4(b). To verify that this new test fixture produced forces on the plate that were similar to the ADL model, a two-exposure hologram was made and its reconstructed image compared with that predicted by the ADL model. Figure 5-5(a) is the reconstructed hologram and Figure 5-5(b) shows the results predicted by the model. The agreement between experiment and the model is excellent. The difference in the number of fringes is due to the fact that the loading was not the same as that used in the model calculation and the contour interval is

larger in the ADL model. The through crack is obvious in both results shown in Figure 5-5.

### 5.3.2 Four-Exposure Moire Experiments With New Loading Fixture

Using the new test fixture, a series of four-exposure moire FLI experiments were designed and performed. The hologram results from one exposure of the plate in the relaxed state and the second exposure with a small torque applied to the new test fixture. The third exposure was formed after a large (about an order of magnitude greater) torque had been added to the small torque already present in the second exposure of the hologram. The fourth exposure of the hologram was made when an additional small torque is added to that already present in the third exposure, and after the object beam had been tilted. This new test fixture was used in a series of experiments. In addition, it was decided to examine the effect of increasing the linear fringe frequency between the third and fourth exposure while keeping all other parameters constant. This effect of increasing linear fringe frequency showed the desensitization of the deformation due to the load with increasing fringe frequency and constituted the breakthrough that renders FLI feasible. The results shown in Figure 5-6 demonstrate that as the linear fringe frequency is increased from Figure 5-6(a) to 5-6(b) to 5-6(c), it is dominating the fringes due to the differential loading, and is making the deformation of the linear fringe due to the crack more visible. Since this effect satisfies the same equation for both two-exposure holographic FLI and four-exposure moire FLI, we next investigated the effect of increasing fringe frequency in two-exposure FLI.

### 5.3.3 Effect of Increasing Linear Fringe Frequency in Two-Exposure FLI

As previously indicated, the restriction on the loading term  $\Delta(x,y)$  in equation (1) was to deformations not greater than one quarter wavelength per linear fringe cycle so that the

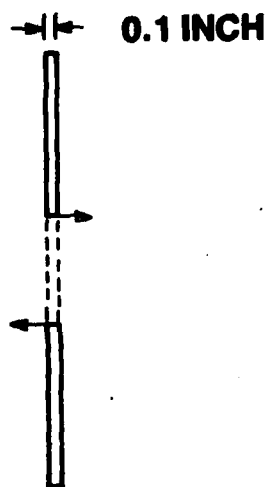


**Figure 5-4(a). Schematic of Forces Created by New Loading Experimental Apparatus**

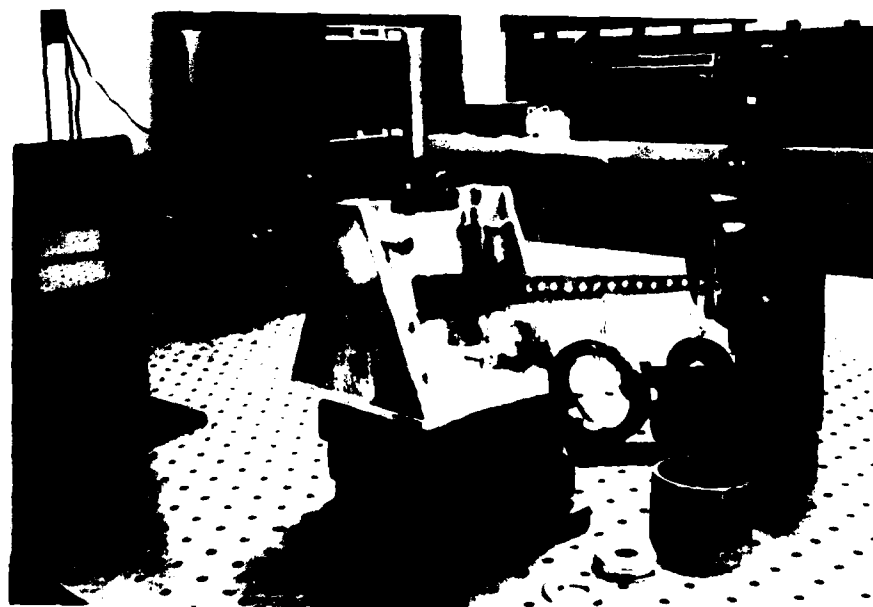


**Figure 5-4(b). Photograph of Loading Apparatus**

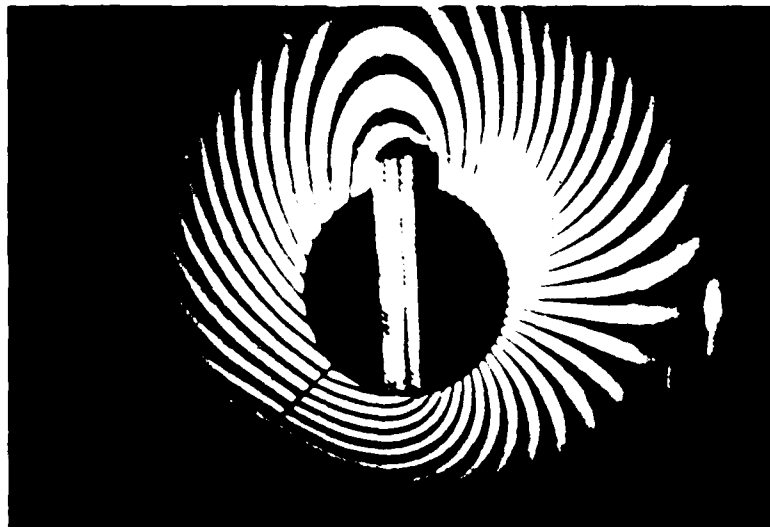


**Figure 5-5(a). Experimental Result**

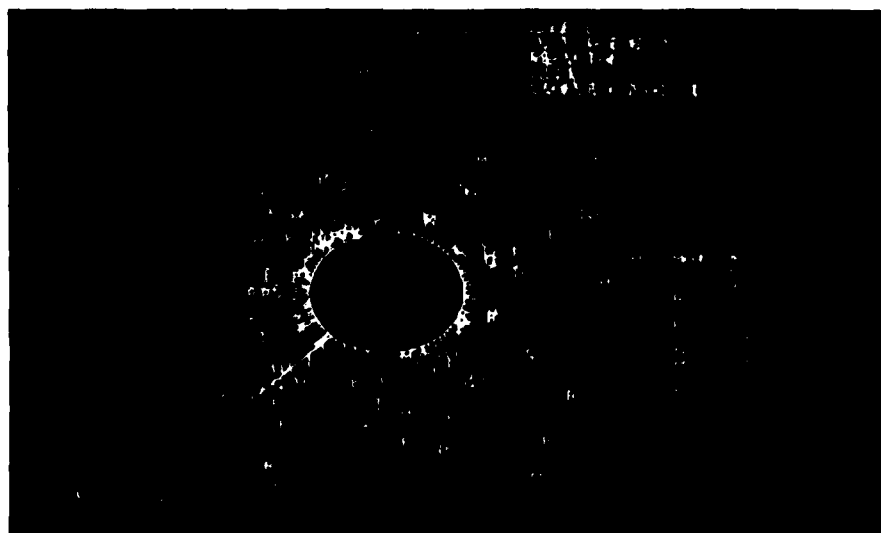


**Figure 5-5(b). Model Prediction**

**Figure 5-5. Comparison of Experimental Result and Model Prediction Using the New Test Plate Fixture**



**Figure 5-6(a).**

Four Exposures

1. Relaxed
  2. 10 ounce-inch torque
  3. 110 ounce-inch torque
  4. 124 ounce-inch torque
- 20  $\mu$ r beam swing  
0.1 cycle/mm



**Figure 5-6(b).**

Four Exposures

1. Relaxed
  2. 10 ounce-inch torque
  3. 110 ounce-inch torque
  4. 124 ounce-inch torque
- 45  $\mu$ r beam swing  
0.25 cycle/mm

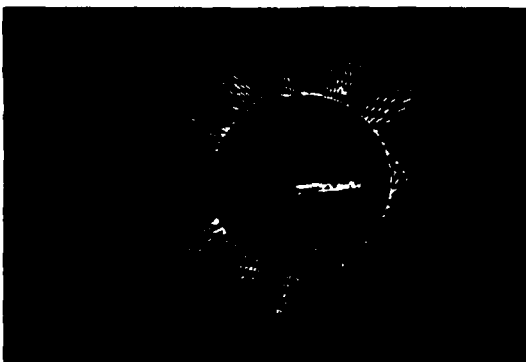


**Figure 5-6(c).**

Four Exposures

1. Relaxed
  2. 10 ounce-inch torque
  3. 110 ounce-inch torque
  4. 124 ounce-inch torque
- 160  $\mu$ r beam swing  
0.9 cycle/mm

**Figure 5-6. Four Exposure Moire Holograms**

resulting vector addition of the  $\omega x$  linear fringe term would not be dominated by the  $\Delta(x,y)$  phase term. The results of Figure 5-6 indicated that we can also satisfy the quarter wave loading constraint by increasing the linear fringe frequency in Eq. 1 so that the load deformation is less than one quarter wave/linear fringe period. This satisfies the quarter wave loading constraint and thereby desensitizes the system. In fact, it should be possible to increase the linear fringe frequency to the point where it dominates the  $\Delta(x,y)$  phase term for a large loading torque and still show a fringe shift at the location of the defect. This should render the two-exposure FLI concept feasible for many practical loading conditions. The ultimate limitation for the frequency for the linear fringes will be determined by the speckle noise in the optical system viewing the hologram. If this limitation yields a non-linear fringe then further desensitization can be achieved by using the more complex two-color, four-exposure moire technique that requires a photograph of the holographic image and a spatial filtering step applied to the image to remove the extraneous moire fringes and create the linear fringes showing the defect location.

#### **5.3.4 Two-exposure FLI Feasibility Demonstration - Desensitization by Increasing Fringe Frequency**

**5.3.4.1 Calibration of Linear Fringe** - The relation between the linear fringe frequency on the object and the angular swing of the object beam was measured. Double exposure holograms were made and the results are shown in Figure 5-7. Figure 5-7(a) shows the object fringe frequency of 0.5 cycle/mm resulting from a 90 micro-radian object beam angle change. Figure 5-7(b) shows that 160 micro-radian swing produces 0.9 cycle/mm and Figure 5-7(c) shows 210 micro-radian swing produces 1.1 cycle/mm. These results are linear within the accuracy of the measurements.

**5.3.4.2 Through Cut** - A series of two-exposure FLI experiments were designed and performed on the test plate with a through cut to demonstrate the desensitization of loading deformation contours by increasing the linear fringe frequency. A two-exposure hologram was made and reconstructed. In each case, the first exposure was for the relaxed state of the test plate and the second exposure was for the stressed state of the test plate with the addition of a linear fringe. The first hologram, shown in Figure 5-5a, shows the deformation from the stress. Figure 5-8 shows the reconstructed image from the double exposure hologram, where, in addition to the stress in state two, a linear fringe has been added. Figure 5-8(a) shows the result when the added linear fringe frequency is low,  $\omega = 0.5$  cycle/mm, on the test plate. The condition of one quarter wave of deformation per fringe cycle has not been met, though the discontinuity at the cut is very visible. Figure 5-8(b) is the result for a fringe frequency of  $2\omega$ , and 5-8(c) is for  $4\omega$ . Figure 5-8(d) illustrates effectively the case of  $8\omega$ . Speckle effects lowered the fringe contrast so the fringes could not be seen. The effect of  $8\omega$  was achieved by reducing the deformation by one half and adding fringes at  $4\omega$ . The fringe shift at the defect is visible at the higher frequencies. This is consistent with goal #1. FLI experiments should reduce holographic patterns as shown in Figure 5-1(a) to those predicted in Figure 5-1(b).

**5.3.4.3 Sub-surface Crack** - Similar experiments were performed on a plate with a sub-surface defect. A test plate similar to the one used for the through cut was made. A 1.16 inch wide saw cut, 3/32 inch deep was made on the back side of the test plate. The cut is 1 inch long, starts at the center hole and is at  $45^\circ$  to the vertical axis. The plate was then subjected to a stress between the exposures. The process was repeated and linear fringes were added by rotating the illuminating beam between the exposures. The results are shown in Figure 5-9. Figure 5-9(a) is the usual interferogram ob-

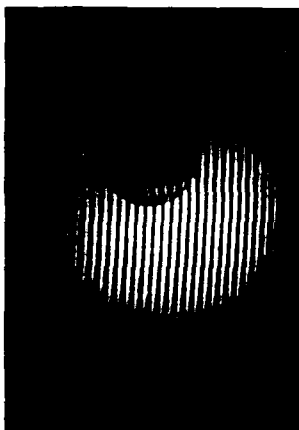


**Figure 5-7(a). Double Exposure**

1. Relaxed
2. 90 microradian Beam Swing  
W = 0.5 cycle/mm on object

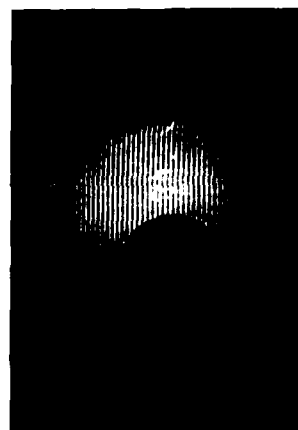


**Figure 5-7(b). Double Exposure**

1. Relaxed
2. 160 microradian Beam Swing  
W = 0.9 cycle/mm



**Figure 5-7(c). Double Exposure**

1. Relaxed
2. 210 microradian Beam Swing  
W = 1.1 cycle/mm

**Figure 5-7. Linear Fringe Calibration of Two-Exposure FLI System**



Figure 5-8(a).  $\omega = 0.5$  cycles/mm



Figure 5-8(b).  $\omega = 1$  cycle/mm

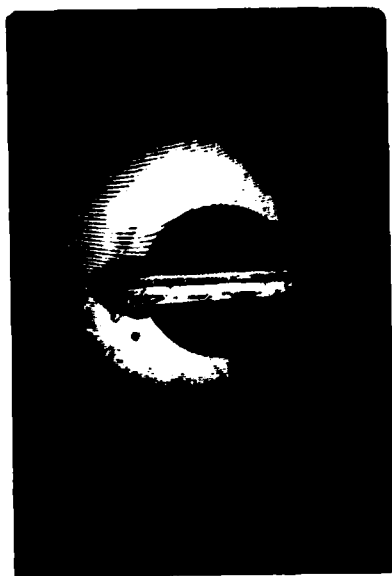


Figure 5-8(c).  $\omega = 2$  cycles/mm

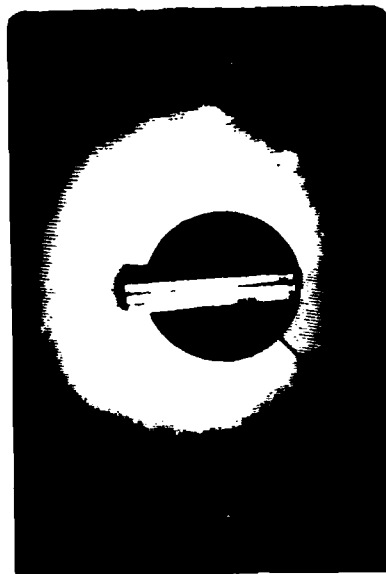


Figure 5-8(d).  $\omega = 4$  cycles/mm

Figure 5-8. Experimental Results of Feasibility for two-exposure FLI for a through cut for increasing linear frequencies.

tained from double exposure holographic interferometry. By carefully examining the photograph, the slight bend of the contour fringes at the cut location can be detected, but the effect is subtle. Figure 5-9(b) shows the interferogram obtained for the same plate stress but with the linear fringe addition. The defect area is quite apparent. This demonstrates the feasibility of the two-exposure holographic FLI technique as predicted in Figure 5-1.

### 5.3.5 Future Directions for FLI

**5.3.5.1 Increasing Linear Fringe Frequency** - The first load desensitization option available in experiments (both static and dynamic) is to increase the linear frequency until the linear fringe is lost in the coherent speckle noise with the two-exposure FLI method. Therefore, we can accept loading forces to the limit where the noise prevents observation of the defect with the linear fringe because the linear fringe is not visible. If this is not sufficient to meet goal #1, then we can further desensitize by using the two wavelength (color) moire method. If color moire is necessary, then spatial filtering will be needed after the holographic reconstruction step to remove the extraneous fringe noise introduced by the technique.

**5.3.5.2 Two Wavelength Moire Desensitization** - The two wavelength moire technique is used to obtain a greater desensitization than is available from increasing the linear fringe frequency in two-exposure holographic FLI to the noise limit. However, this complicates the process. The two holograms of the four-exposure moire holographic method are made with two different lasers (wavelengths),  $\lambda_1$  and  $\lambda_2$ . The moire fringes are of the form

$$\cos(\omega x + \Delta K \Delta \phi) \quad (2)$$

where  $\Delta K = 2\pi (1/\lambda_1 - 1/\lambda_2)$  and  $\Delta \phi$  is the path difference (out of plane surface deformation), caused by the differential loading between the two moire holographic exposures. From equation (2), which is similar to the two-exposure

FLI equation given by equation (1), we note the increase desensitization from the term  $(\Delta \phi K \Delta)$  which is equivalent to the  $\Delta$  term in equation (1). Now, because of the utilization of the two wavelengths, we can make  $\Delta k$  a very small number and the effective  $\Delta \phi$  much larger while still keeping the product small, which will retain the full desensitization effect of increasing the linear fringe frequency. Thus, the four-exposure moire technique with two wavelengths gives an additional desensitization to that obtained by increasing the linear fringe frequency. The limitations of this process will be investigated during the next reporting period.

### 5.4 FINITE ELEMENT MODELING FOR DETECTION OF A PART-THROUGH CRACK

The superposition of linear fringes proved invaluable in the isolation of the holographic signature of both a through cut and a sub-surface cut in an aluminum plate. The same plate configuration with the same loading mechanism is modeled in this section using finite element analysis. The analyses show the importance of linear fringe for detecting and locating defects.

The analyses described were performed using the general purpose finite element code ANSYS. The plate was broken into finite elements, indicated in Figure 5-10. The mesh is finest in the region of the crack emanating from the central hole; the crack tip is at the corner of the three quadrilaterals that meet in a "triple point." An extremely fine layer of elements exists along the crack; this layer of elements was assigned a thickness of 0.01 inches to model the ligament of the sub-surface crack. The remainder of the plate was 0.1 inches thick, as in the experiments. The elements were also assigned a Young's modulus of  $10 \times 10^6$  psi and a Poisson ratio of 0.34, characteristic of aluminum. The plate was loaded by equal and opposite forces of 4 pounds at the top and bottom of the hole. This loading corresponds to a moment of 4 inch-pounds, and it closely models the loading mech-

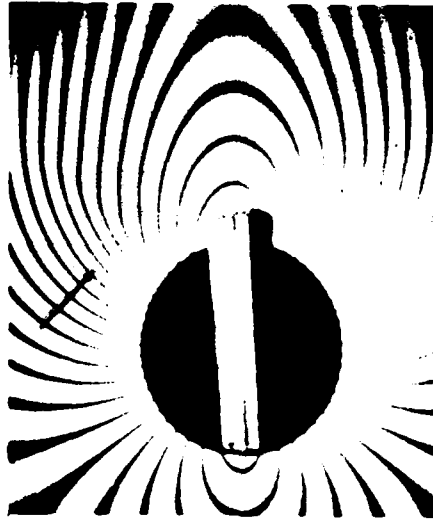


**Figure 5-9(a). No linear fringe in two-exposure holography**

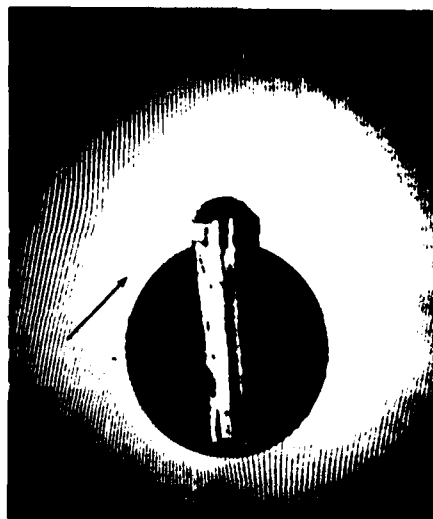


**Figure 5-9(b). Linear fringe in two-exposure FLI**

**Figure 5-9. Double-exposure Holography of a test plate containing a sub-surface crack with and without linear fringes demonstrating the feasibility of the FLI method.**

anism used in the experiments. The plate was clamped on three sides and free on the fourth side.

In fringe linearization holography, the object beam is tilted between holographic exposures to create linear cosine fringes in the reconstructed interferogram. To model this effect in the finite element analysis, the plate is given a rigid rotation corresponding to the object beam

rotation. As in the case of the object beam, a rotation that is too great will completely swamp the important features of the deforming structure, and in particular, a flaw signature could become undetectable. In the following results, a set of increasing rotations was tried until the desired result was achieved.

Figure 5-11 shows the model results, which are contours of out-of-plane displacement, for the

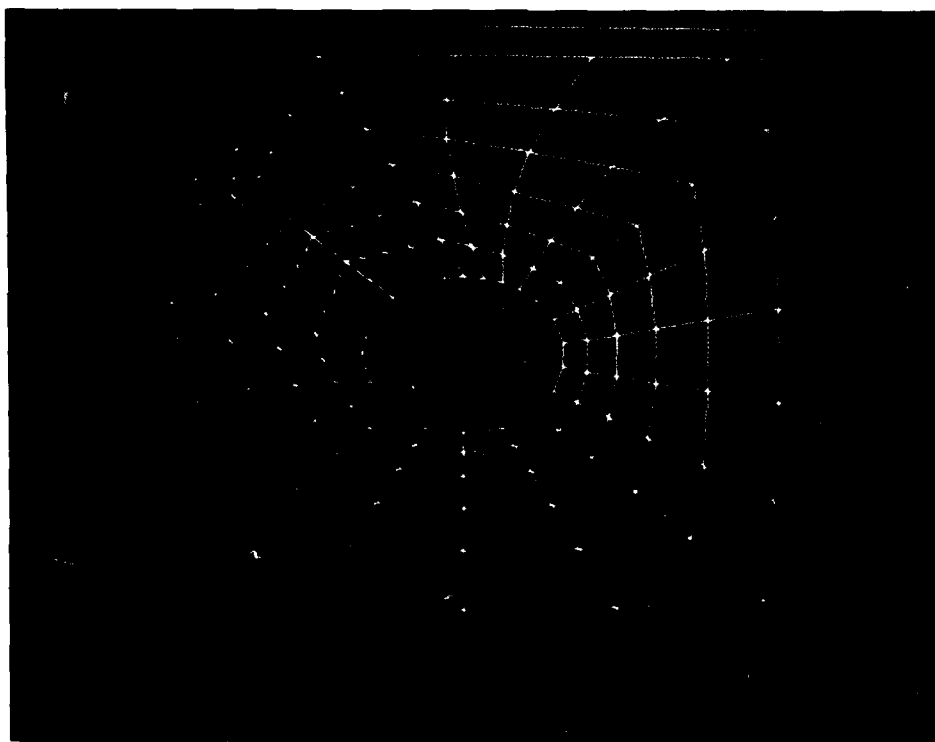


**Figure 5-10. Finite Element Mesh for Analysis of Cracked Specimens. Crack Tip is at the "Triple Point" in the Third Quadrant.**

case with no linear fringes. The slight hash mark at 10 o'clock shows the extent and orientation of the part through crack, the other end of which is at the hole. The experimental model subsurface crack, a saw cut, is one inch long and perpendicular to the circular hole,  $45^\circ$  from vertical. While a discontinuity in the slope of the contours can be noted at the crack, the crack signature by no means dominates the contour map. Other discontinuities in contour slope arise due to the discrete nature of the finite element mesh. Linear fringes were then added, corresponding to a rigid rotation of the model plate equivalent to a rotation of the beam illuminating the model plate.

Figures 5-12, 5-13, and 5-14 correspond to an in-

crease in the amount of rotation from 0.2 milliradians to 2.0 milliradians. In Figure 5-12, the dashed line (corresponding to the median displacement level, zero here) which was horizontal in Figure 5-11, has begun to rotate clockwise, indicating the presence of the linear fringes. Unfortunately, however, the location of the part through crack is still not completely obvious. In Figure 5-13, the rotation is increased to 0.5 milliradians, and the linear fringes are beginning to dominate. Nevertheless, the discontinuity in slope at the part through crack shows up quite clearly. In Figure 5-14, where the rotation is 2 milliradians, the linear fringes have overwhelmed almost all features of the deformed plate except for the high gradients existing at the part through crack.

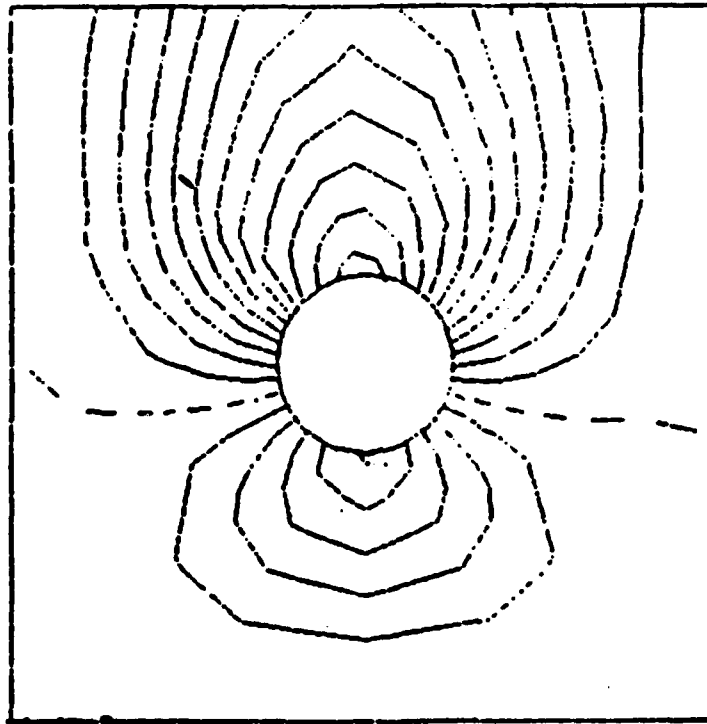


**Figure 5-11.** Computer model of stressed plate. Plate has subsurface crack. Defect extends from hole to hash mark at 1:30 contours are at 12 micron surface displacement intervals.

This figure corresponds almost exactly to the interferogram shown in Figure 5-9b.

As a result of the modeling efforts, it is felt that linear fringes provide an effective tool for isolating the holographic signature of a particular defect. Rigid rotation of the body, corresponding to a shifting of the object beam in holography, must be selected judiciously so as to eliminate the clutter in the interferogram without destroying the discontinuities that signify the presence of a flaw. Rules for calibrating this rotation will be determined during the next re-

porting period.

## 5.5 POTENTIAL FOR AUTOMATIC READOUT

The linear fringe in the two-exposure holographic FLI (or four-exposure, two-color, holographic moire) readily lends itself to using an automatic readout, the second goal to be accomplished. Although this has yet to be implemented, we present conclusive evidence that effects are present at the defect site in the linear fringe holographic reconstruction which

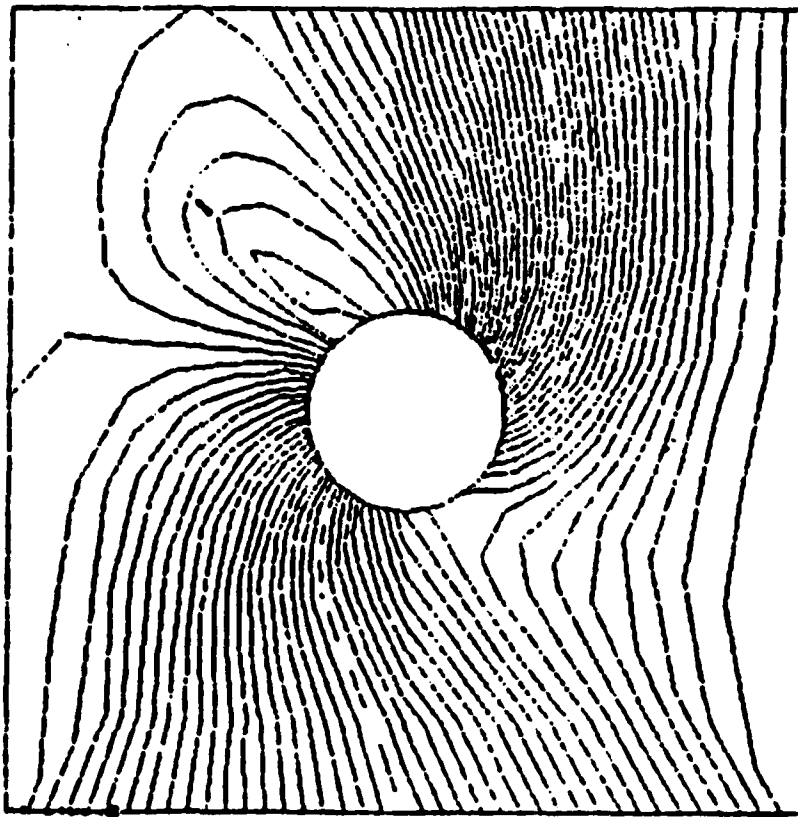


**Figure 5-12.** Computer model of plate in Figure 11 with addition linear fringes due to a 0.2 milliradian plate rotation.

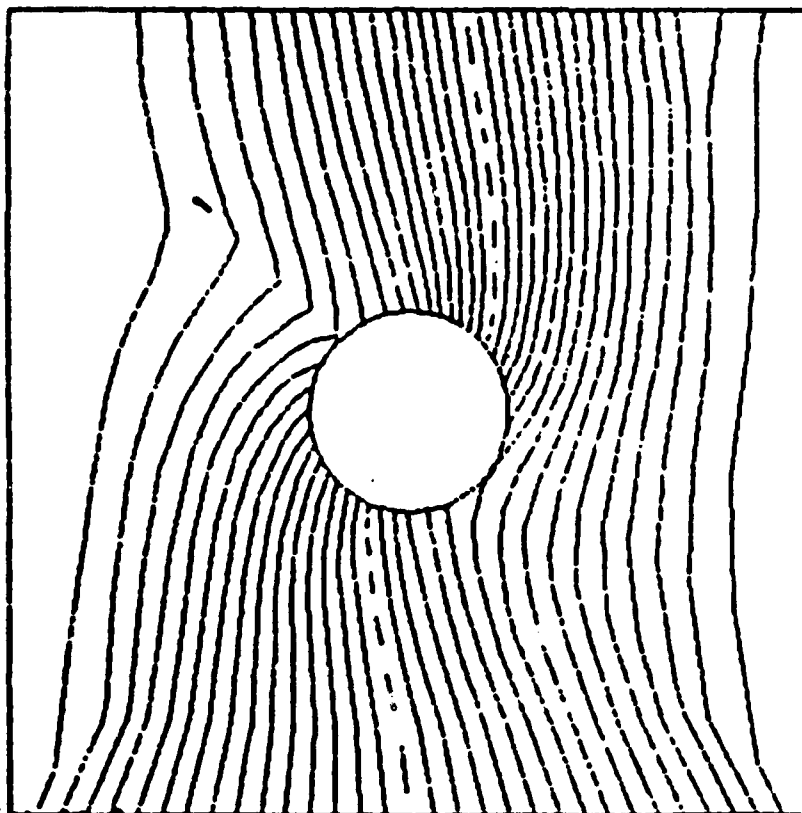


**Figure 5-13.** Same as Figure 5-12, with plate rotation increased to 0.5 mr.

can be detected and used for the automatic readout. To show these effects, we use a diffractometer, a two-dimensional optical spatial Fourier transforming system. In Figure 5-15, we show the diffraction pattern from parts of the reconstructed image of a two-exposure FLI hologram at a defect free region and at the site of the through cut shown in Figure 5-8(d). Figure 5-15(a) shows the Fourier signature of the linear fringe (diffractometer was at region to left of defect). We recognize the d.c. term and the two first orders of the linear fringe transform. In Figure 5-15(b), we see the signature at the defect sight (the through cut). The fringe shift

at the cut location results in a different d.c. term and two sets of first-orders for the two linear fringes at the cut. The diffractometer outputs clearly show there exists a signature at the defect site distinguishable from the defect free region.

Figure 5-16 shows the diffractometer output for a subsurface cut. In Figure 5-16(a) we see the signature for a defect free region of Figure 5-9(a), and in 5-16(b) the signature at the defect region of Figure 5-9(b).

This demonstrates that measurable and detectable results characterize defects present in FLI

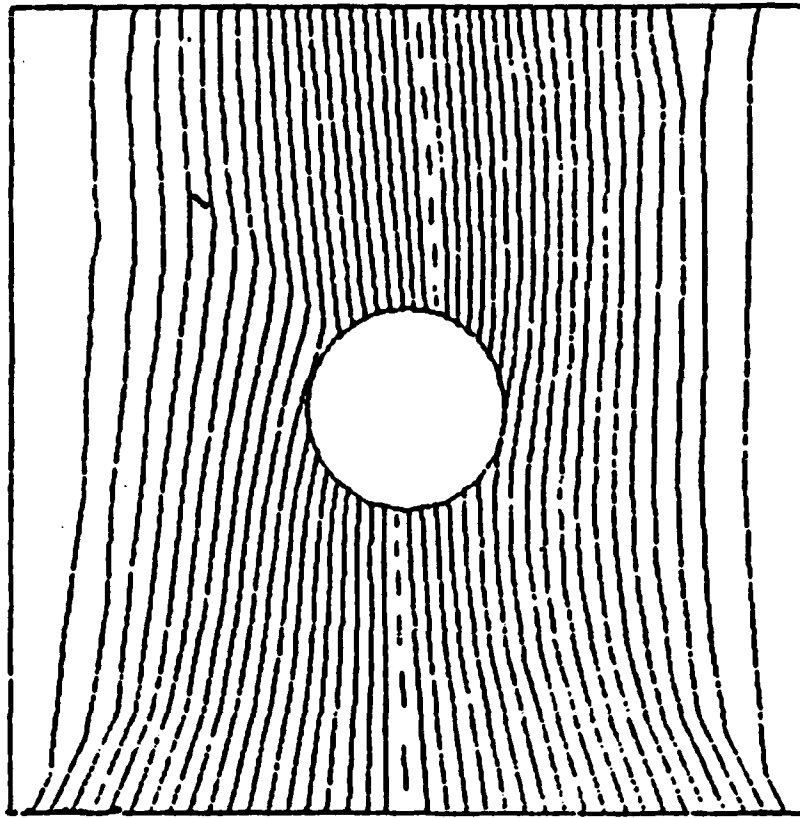


**Figure 5-14. Same as Figure 5-12, with plate rotation increased to 2.0 mr. Subsurface cut is revealed by bending linear contour lines.**

detection. These effects can be exploited in the development of an automatic readout system.

The most likely method for doing this would be to go to the reconstructed image plane of the two-exposure FLI hologram and introduce an image processing algorithm for scanning the

linear fringes to determine the presence of the defect. Alternatively, we can record the reconstructed image from the two-exposure FLI hologram and use a diffractometer (as already shown) to exploit the defect detection. Thus, goal #2 appears attainable with two-exposure FLI holography.

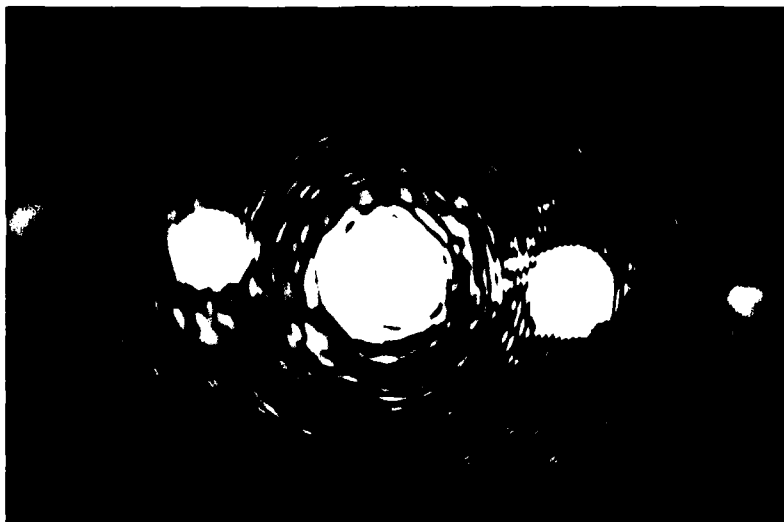


**Figure 5-15(a). Linear**

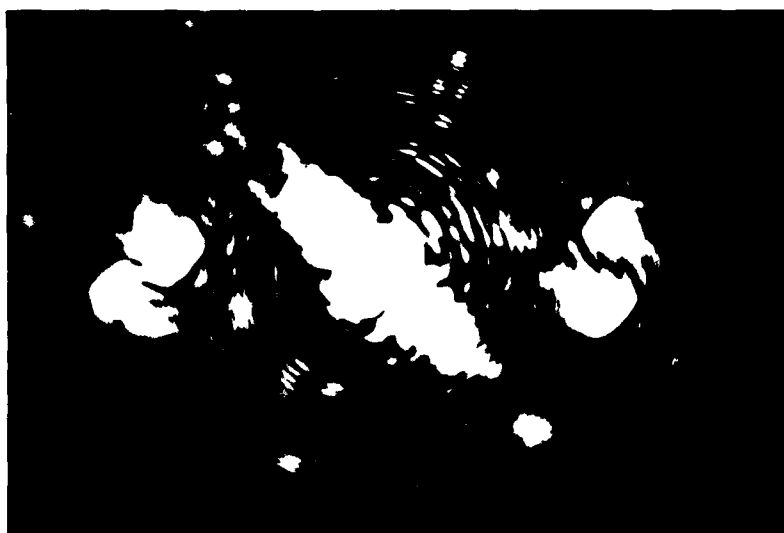


**Figure 5-15(b). Cut**

**Figure 5-15. Diffractometer Readout from Nearly Linear Fringes at Highest Frequencies for Through Cut**

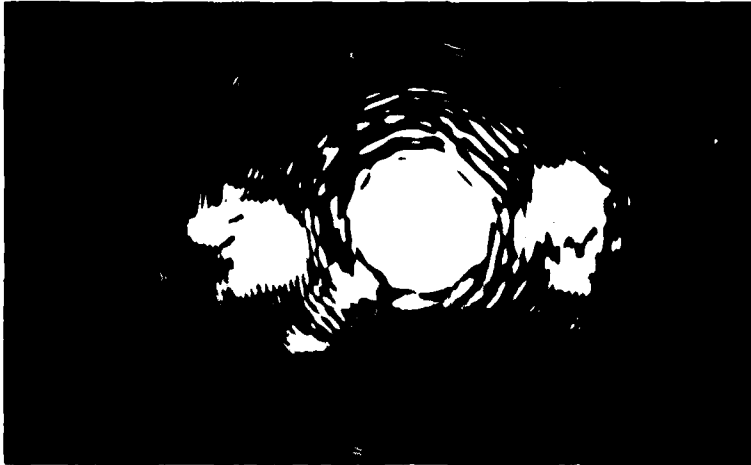


**Figure 5-16(a). Linear**



**Figure 5-16(b). Cut**

**Figure 5-16. Diffractometer Readout from Nearly Linear Fringes at Highest Frequencies for Sub-surface Cut**

## SECTION 6 RESULTS TO DATE

Results obtained during this reporting period were significant as they demonstrated the experimental feasibility of the FLI concept.

- It was determined that significant desensitization of the random fringe moire is achieved by increasing the linear fringe frequency (angular tip of object beam when making the hologram).
- A new fixture was made that closely resembled the model.
- Experimental results showed linearization of fringes and location of both a through cut and a sub-surface cut.
  - no spatial filtering required.
- Highest possible frequency will be limited by the speckle noise of holographic imaging system.
- Further desensitization, if necessary, can be achieved by using the two-color, four exposure holographic moire technique
  - Spatial filtering will be required.
- Modeling effort also showed cut detection with increased frequency fringe linearization and is in excellent agreement with the experimental results.
- Experiments with a Fourier diffractometer showed that both the through cut and the sub-surface cut had Fourier signatures significantly different from those of the defect free area fringe.
  - Automatic readout techniques are possible with such characteristic signatures using image processing software or the Fourier method.

## SECTION 7 FUTURE PLANS

In the time remaining on this program, we will complete as many of the following tasks as possible.

- Determine optimum linear fringe frequency as a function of surface displacement
  - Model
  - Experiment
- Sensitivity Analysis
  - Sub-surface crack location
  - Magnitude of forces needed
  - Size and depth of crack signatures
  - Experimental verification of computer model
- Desensitization by
  - Fringe frequency increase
  - Two-color moire
  - Frequency increase plus two-color moire
- Model Dynamic Forces
  - Estimate maximum excursions at defect as function of input forcing function and frequency content
- Design and perform a small area dynamic force experiment to locate sub-surface crack
  - Use the Honeywell Argon CW Laser

## **SECTION 8 REFERENCES**

1. TRW Systems Group, "Feasibility Demonstration of Applying Advanced Holographic Systems Technology to Identify Structural Integrity of Naval Aircraft," Interim Report on Contract No. N62269-72-C-0400, 23 March 1973.
2. Metals Handbook, Vol. 11, "Non-destructive Inspection and Quality Control," American Society of Metals, Metals Park, Ohio (1976) p. 215.
3. N. Abramson, "The Making and Evaluation of Holograms," Academic Press, N.Y. (1981) p. 222.

**END**

**FILMED**

**1-85**

**DTIC**